Food Biophysics (2012) 7:15–27
DOI 10.1007/s11483-011-9238-8

ORIGINAL ARTICLE

Power Laws in the Elasticity and Yielding of Plant Particle Suspensions

Patricia Lopez-Sanchez · Robert Farr

Received: 31 January 2011 / Accepted: 27 September 2011 / Published online: 5 October 2011

Abstract The yielding and flow behaviour of plant suspensions are perhaps the most important rheological properties in process and product design for applications in paper, biofuel and food industries. Studies are reported here on the yield properties and flow behaviour of suspensions of plant particles with different shapes (clusters of cells, individual cells and cell fragments). Carrot and tomato were selected as model plant systems to prepare suspensions at particle dry mass concentrations ranging from 0.010 to 0.065. The flow behaviour was characterised by an apparent yield stress and shear thinning. The Herschel-Bulkley yield stress obtained from up and return flow curves was compared to the yield stress calculated from oscillatory measurements. The dependence of the yield stress values on particle dry mass concentration is approximately a power-law, with a fitted exponent of 3±0.5 for all the suspensions, independently of the plant origin and particle shape. This same power-law behaviour was found for the elastic modulus G′, and in this case the exponent was 3 for carrot and 4 for the tomato suspensions. The yield strain, calculated from oscillatory measurements, decreased slightly with dry mass fraction, but did not follow a power-law. We discuss possible explanations for power law behaviour, and provide a model for G′ based on folded elastic sheets, which predicts an exponent of 3, similar to the values obtained for these suspensions.

Keywords Yield stress · Yield strain · Power-law · Rheology · Elastic modulus · Plant · Suspension · Carrot · Tomato

P. Lopez-Sanchez (✉)
Structured materials and process science, Unilever R & D,
Olivier Van Noortlaan 120, PO Box 114, 3130 AC, Vlaardingen,
The Netherlands
e-mail: patricia.lopez-sanchez@unilever.com

R. Farr
Unilever R&D,
Colworth Science Park, Sharnbrook,
Bedford, UK

R. Farr
London Institute for Mathematical Sciences,
22 South Audley Street, Mayfair,
London, UK

Introduction

Suspensions of plant material are common products or by-products in many industries, such as paper, biofuel and food. These suspensions are in general highly polydisperse in particle size, shape and in chemical composition. In conventional food processing, the plant tissues are disrupted, and the resulting structures such as clusters of cells, individual cells, and cell fragments are suspended in a liquid medium composed of water, sugars and organic acids, amongst other solutes. The suspended plant particles can be thought of as elastic objects composed of mainly cell wall material, a composite of cellulosic and non-cellulosic polysaccharides (mainly pectin). The complex nature of the plant particles makes it difficult to link the rheological behaviour of these suspensions and the physical properties of the particles (volume fraction, particle shape and deformability) and to determine which type of interactions such as hydrodynamic, frictional and collisional forces between the particles determine the material behaviour.

In general these types of suspensions of plant material exhibit a yield stress[1] and have solid viscoelastic behaviour below the yield stress, whereas above the yield stress they flow. The origin of the yielding behaviour is difficult to

determine since in these plant suspensions, as described above, many factors may operate simultaneously, and it is not clear which is the dominant at a given particle concentration. In principle the suspensions will display a yield stress when a certain particle concentration is reached and a percolating network is formed. Below this concentration the particles will not be space-filling and hence the system has no yield stress. Once a percolated network is formed the particles are not free to slide past one another under small strains, but instead must be forced to deform in order to accommodate the imposed strain. It has been previously hypothesised that provided interactions between particles such as steric interactions, electrostatic forces and adhesion from attached polymer chains are all short-ranged, it is the elastic energy of deformation of the particles which generates the stress during slow deformation up to yielding (hence G′), and the rupture of this network sets the yield stress.[2] Viscosity (and G″) on the other hand can arise from viscous deformation of the liquid phase (long range hydrodynamics or lubrication forces between particles), or direct sliding friction between the particles.

Several theoretical models have been developed to predict viscosity as a function of phase volume,[3] for example the Einstein equation predicts the viscosity of extremely dilute hard spherical particles, while somewhat higher volume fractions are captured in the Batchelor model, which includes particle-particle and particle-medium interactions. More advanced models, like the Krieger-Dougherty include the maximum packing fraction ϕ_{max}, defined as the solids content which makes suspension flow impossible for undeformable particles. However measuring the phase volume of soft, highly deformable plant particles is very challenging. Even if the phase volume is accepted as a well-defined concept (which is not always clear), the maximum packing fraction can only be estimated theoretically when particle attributes such as shape and size distribution are exactly known. Therefore the predictive application of such models to plant suspensions is extremely difficult and models based on particle concentrations, rather than particle phase volume, have been empirically developed.[4–7] However due to the influence of plant variety, and the different processing conditions used in those studies there is not yet available a model to describe the standard behaviour of such plant suspensions as a function of particle attributes.

The main objective of this work was to study the yield and flow behaviour of plant particle suspensions with different shapes such as cell clusters, individual cells and cell fragments, as a function of particle concentration. Carrot and tomato were selected as plant model systems. Herschel-Bulkley yield stress was obtained from shear rate ramps while yield stress and strain values were calculated from oscillatory measurements. An improved understanding of the complex rheological behaviour of plant particle suspensions could aid in the design of manufacturing processes to optimise the material properties of products structured mainly with plant material.

Materials and Methods

Preparation of Model Plant Suspensions

Fresh carrots (*Daucus carota*, var. Nantes) and salad tomatoes (*S. lycopersicum*) were purchased from a local supermarket and stored at 5 °C prior to processing. The vegetables were thoroughly washed.

Particles with different shapes were prepared based on the methods described in our earlier studies.[8] To obtain clusters of cells the carrots were peeled and cut into approximately 1×1×2 cm pieces. The carrot pieces were mixed with de-ionised water at 1:1 ratio. The sample was placed in a stainless steel vessel for quick heat transfer. The vessel was kept in a hot water bath which was maintained at 90±5 °C, and covered to prevent losses due to evaporation. Thermocouples were attached to three carrot pieces to check that the desired temperature of 90±5 °C was reached in the core of the pieces, and then the vessel was heated, while stirring, for 40 min. After thermal treatment the mechanical disruption was done using a kitchen blender (model 5KSB52, Kitchen Aid, Michigan, USA) at its maximum speed for 3 min. Individual cells were prepared from tomato following a similar process with some minor modifications: stem and core were removed and the tomato:water ratio was 9:1 due to the amount of unbound water naturally present in this fruit. The resulting tomato suspension was sieved through a 1 mm pore size sieve to remove seeds. Cell fragments, with a compact or open structure, were prepared from the resulting carrot and tomato suspensions using a high pressure homogeniser (Panda 2 k, Niro Soavi, Parma, Italy) in its standard configuration via a single pass at 60 MPa.

In order to have standardised dispersed particles in sufficient amount the carrot suspensions were weighed in several large flasks and centrifuged at 3500 rpm equivalent to 1976 g (Centrifuge Beckman Avanthi JA-12, CA, USA). The particle size and morphology of the particles were not significantly affected at this centrifugation speed. The supernatants were removed and dilutions were prepared from the wet sediment. In the tomato suspensions there were enough solids present, therefore the dilutions for tomato were prepared from the initial suspension without centrifugation. Deionised water was used for preparing the carrot and tomato dilutions, due to the low contribution of the serum phase to the overall rheology,[8] covering a range of particle dry mass fractions from 0.010 to 0.065. Particles

were gently mixed with water and the resulting suspensions were left to stabilise overnight (kept at 5 °C).

Characterisation of the Model Plant Suspensions

Measurement of the Dry Mass Fraction

Dry mass fraction *w*, was defined as the mass of a dried sample divided by its initial wet mass. Dry mass fraction was determined by drying 5±0.2 g of each sample in a vacuum oven (Memmert GmbH+Co. KG, Schwabach, Germany) at 70 °C and a pressure of 4 KPa for 5 h. The dry mass fraction was calculated, in triplicate, from the sample weight before and after drying.

Measurement of the Particle Size Distribution

The particle size distribution was measured using light scattering (Mastersizer, Malvern Instruments Ltd, Malvern, UK). Approximately 0.5 mL of each sample was pipetted into a water-continuous diluting accessory (2000 Hydro-S) filled with 1000 mL of deionised water. The particle size distribution was calculated from the intensity profile of the scattered light using the instrument software (Mastersizer 2000, version 5.40). The area-based ($d_{3,2}$) diameters were obtained for every sample.

$$d_{3,2} = \sum_i n_i d_i^3 / \sum_i n_i d_i^2 \quad (1)$$

Where n_i is the number of particles of diameter d_i.

The measure $d_{3,2}$ was selected for the average particle size of the dispersions because in systems with a broader particle size distribution, like the ones in this study, the volume based particle size parameter $d_{4,3}$ will be highly influenced by large particles, whereas the area-based $d_{3,2}$ is less weighted towards large particles, and thus can be more sensitive to the fraction of smaller particles present. It is also worth noting that in the systems under study, these values, based on light scattering, which assumed spherical particles, should be treated with caution, as the particles in the dispersions are certainly not exact spheres, and in the case of cell fragments, may have large aspect ratio. Therefore, throughout this paper, "diameter" will refer to twice the radius of gyration of a particle.

Light Microscopy

Light micrographs were taken using a Zeiss Axioplan microscope (Zeiss, Carl Zeiss Ltd, Hertfordshire, UK) equipped with a video camera (Qicam Fast 1394, Qimaging, Surrey BC, Canada). The samples were diluted twenty times with deionised water and slowly mixed. Two droplets were placed on a glass slide and covered. The samples were observed with a 10× dry objective lens using the differential interference contrast mode (DIC). At least 6 images were obtained per sample. The software Linksys 32, version 1.9.6 (Linkam Scientific Instruments Ltd., Tadworth, Surrey, UK) was used to control the camera and collect size-calibrated images.

Rheology Experiments and Data Analysis

The rheological measurements were carried out using a stress controlled rheometer (ARG2, TA Instruments, Delaware, USA) which was equipped with a 4 blade vane[9] and a cup with roughened surfaces to reduce slip at the walls of the rheometer. The vane tool was selected based on literature data as the best system to reduce or eliminate wall slip in viscoelastic particulate systems which are particularly vulnerable to this phenomenon (other advantages of this geometry include less disturbance of the sample on inserting the measurement probe, fewer problems with large particles and easy sample loading)[9]. The vane had a diameter of 12.6 mm and a height of 42.5 mm, the diameter of the cup was 30 mm. The gap was 8.7 mm, working with this wide gap allows the study of systems with large particles ensuring that for all the suspensions there were enough particles in the gap to consider that we measure the properties of a continuum medium. All measurements were performed at 20±0.1 °C maintained with a Peltier system. Approximately 50 mL of sample was loaded into the rheometer. Three measurements per sample were carried out. The rheology of these types of materials is sensitive to microstructural arrangements of particles and thus to the initial configuration, therefore the suspensions were pre-sheared before starting the oscillatory experiments at 100 s^{-1} for 60 s followed by a resting step of 5 min.

Following the pre-shear, the oscillatory shear experiments were carried out. A strain γ sweep from 0.01 to 300% strain was performed at a frequency of 1 Hz. The oscillatory measurement allows determination of the yield strain γ_y in an accurate way because the departure from the linear regime is controlled. The yield strain of the suspensions was calculated in the following manner: it was found that the functional form of Equation 2 provided a good fit to the strain amplitude (γ) dependent oscillatory elastic modulus G′ at a frequency of 1 Hz:

$$G' = G_0' \exp\left(-A\gamma^B\right) \quad (2)$$

Where G_0' is the limiting modulus at zero amplitude, and A and B are constants. At large deformations the measurements might be influenced by other phenomena happening in the rheometer leading to unreliable measurement points, therefore points below half the plateau value of G′ were not considered for the fitting. The yield strain, γ_y was

determined by finding the amplitude at which G′ has fallen to 90% of its value at zero amplitude as shown in Equation 3 (which follows directly from Equation 2).

$$\gamma_y = \left(\frac{\ln(100/90)}{A}\right)^{1/B} \quad (3)$$

From the oscillatory measurements a yield stress, $osc\sigma_y$, was also calculated as the yield strain times G′ (Equation 4).

$$osc\sigma_y = G'\gamma_y \quad (4)$$

Measurement of the steady-state shear dependent viscosity of the suspensions was conducted by increasing the shear rate from 0.01 to 100 s^{-1} and back during a total time of 4 min. Performing a yield stress measurement is challenging and there are several methods designed to evaluate the yield stress of this type of materials.[10] The rheometer software (Rheology advantage, v5.7.0, TA instruments, Delaware, USA) was used to obtain the yield stress, σ_y, values by fitting the up and return curves to the Herschel-Bulkley model (Equation 5):

$$\sigma = \sigma_{yield} + k\dot{\gamma}^n, \quad (5)$$

where σ is the stress and $\dot{\gamma}$ the shear rate, k and n constants. For the measurement points at low shear rates, only a small total strain was applied to the sample, and it is doubtful whether a steady state measurement has been achieved. Therefore only measurement points corresponding to an applied strain of more than 1 were retained for the fitting procedure. Furthermore a calibration with silicon oil was done to calculate the Reynolds number above which inertial effects might play a role; values above a Reynolds number of 3.5 were not considered for the fitting.

Results

Particle Characterisation

An overview of the shape and size of the particles studied is given in Figure 1 and Table 1. The carrot cell clusters had an average diameter of 103 μm and the carrot cell fragments of 50 μm. Even though most of the particles could be described by those shapes and sizes the suspensions were polydisperse to a certain degree (Figure 2), for example some small clusters were still present in the

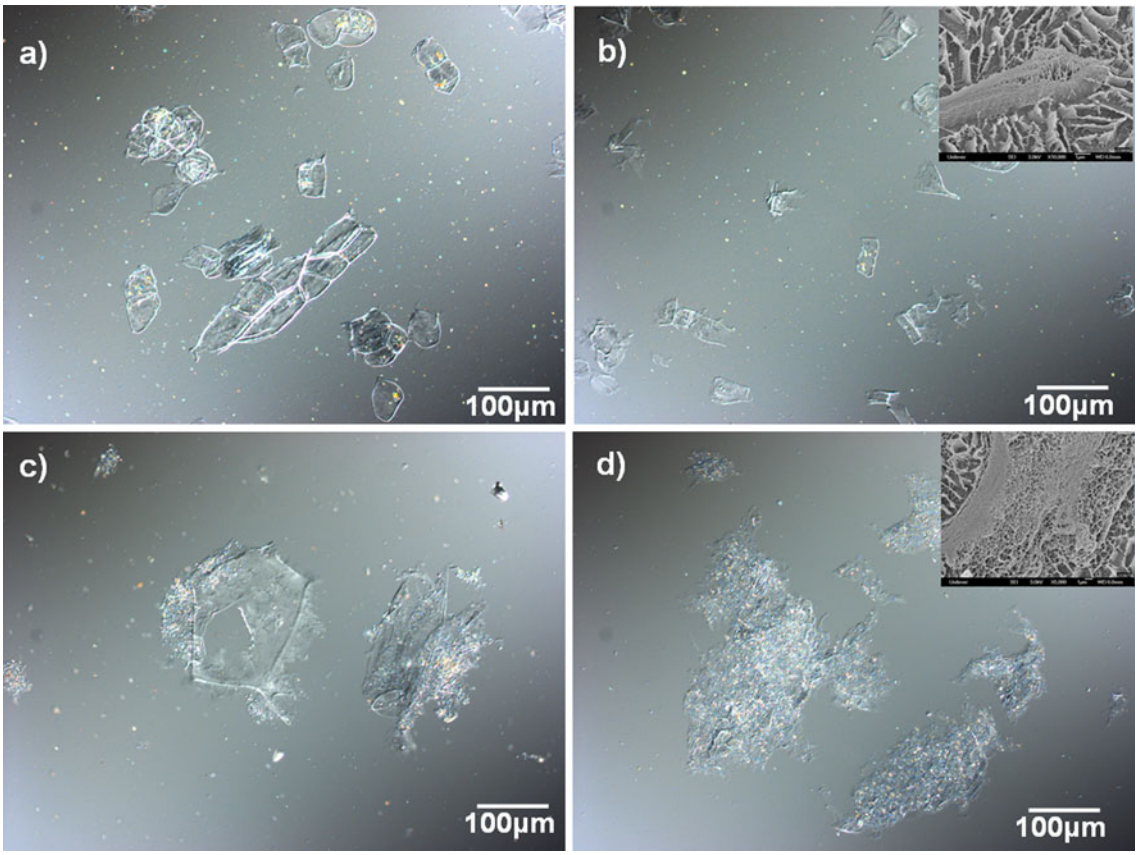

Fig. 1 Optical micrographs showing particle morphology (**a**) carrot cell clusters, (**b**) carrot compact cell fragments, (**c**) tomato individual cells and (**d**) tomato open cell fragments. Cryo-SEM micrographs (scale bar 1 μm) are included as an inset, they show the compact nature of the carrot cell wall and the swelling of the tomato cell wall (Images from Reference[8])

Table 1 Area-based diameter $d_{3,2}$ of carrot and tomato particles

	Carrot		Tomato	
Particles	cell clusters	compact cell fragments	individual cells	open cell fragments
$d_{3,2}$ (μm)	103±1	50±5	233±6	107±6

suspension of cell fragments. The average diameter of the tomato individual cells (mainly intact) was 233 μm. Cryo-SEM micrographs (inset in Figure 1b and c) showed that the tomato cell fragments had a more open structure than the carrot fragments. It has previously been shown[8,11] that after a thermal treatment tomato cell walls start to be disrupted, leading to expansion of biopolymers into the liquid phase, and this swelling of the cell walls is increased by high pressure homogenisation. The dilution, required for light microscopy observation, led to amorphous structures, likely a mixture of cell content and cell wall material, which are believed to form a continuous network rather than being individual particles,[11] therefore measuring the particle size of such a suspension is meaningless. Suspensions containing these four types of particle shapes: cell clusters, individual cells and two types of cell fragments with compact and open cell wall structure, were studied.

Flow Properties

The effect of particle concentration on the flow behaviour is plotted in Figure 3 in the form of viscosity as a function of shear stress. All suspensions showed a qualitatively similar flow behaviour, independently of the plant type and particle shape. In Figure 3, curves corresponding to suspensions of carrot cell clusters are shown. The up and return curves agreed very well provided that a strain of at least 1 was applied to the sample in the course of a single rheological measurement point. This indicates that very little damage to the structure has occurred as a result of the first up-sweep rheological measurement. However the data for the first measurement points of the rheological up-sweep were noisy, probably due to the sample being subject to insufficient strain for a steady state to have been adequately achieved. This was not the case in the return curves. The suspensions exhibited an apparent yield stress and shear thinning behaviour, the viscosity decreased with shear stress, over the entire studied concentration range. No low shear rate plateau in the flow curves was detected, the detection of such a plateau is rather difficult due to the presence of both elastic and flow behaviour at low stresses. Similarly the presence of a high shear plateau was not clearly measured. Dispersions with a dry mass fraction below 0.015 showed particle sedimentation and it was not possible to measure them with the current method. Above a w of 0.044 the solid nature of the sample led to irreproducible measurements with the vane geometry.

Yield Stress and Elastic Modulus

In this work the apparent yield stress σ_y was calculated from steady-state and oscillation measurements. The up and return flow curves were fitted to the Hershel-Bulkley (HB) model (Equation 5). The fitting error varied between 5–20% for all suspensions. The largest error was for the up curves; a more conservative selection of the minimum strain i.e γ=10 could improve the fitting. The Hershel-Bulkley flow index for the highest and lowest concentration

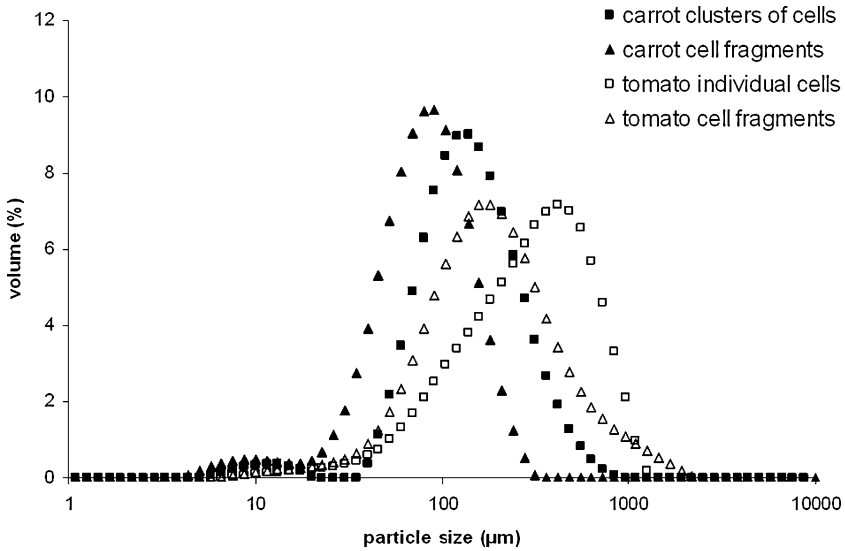

Fig. 2 Typical particle size distributions of carrot and tomato particle suspensions

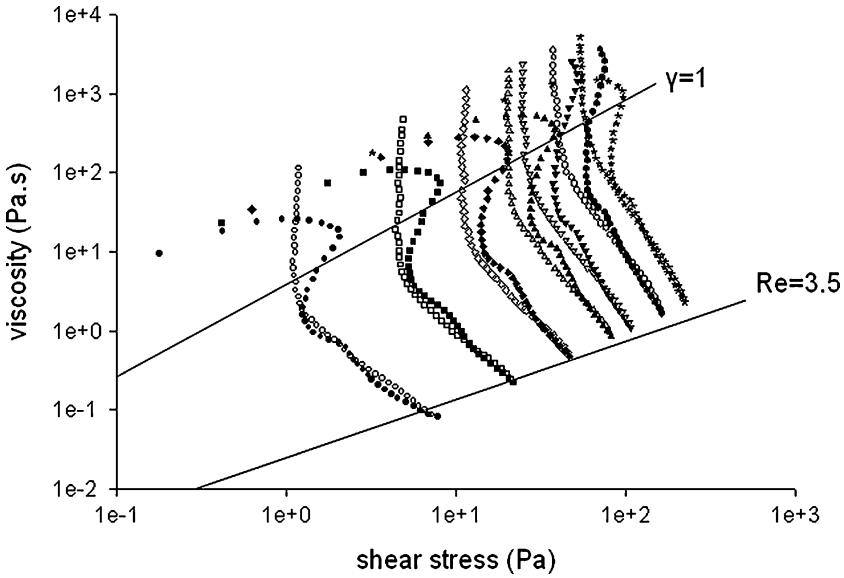

Fig. 3 Concentration dependence of flow curves for suspensions of carrot cell clusters. Up curves (closed symbols) and return curves (open symbols). Solid lines mark the limits used for data analysis and fitting to the Hershel-Buckley model: a minimum strain of 1 and a maximum Reynolds number of 3.5. From left to right: particle dry mass fraction w increases: 0.015, 0.020, 0.025, 0.029, 0.034, 0.039, and 0.44

samples of each data series are shown in Table 2. The values from the return curves appear to be more reliable as the Herschel-Bulkley model provides a good fit to the data in these cases. The index lies in the range 0.2 to 0.35 for the return curves (and is somewhat larger for the up-curves). From oscillatory experiments yield stress and yield strain were calculated as described above (Equations 2–4). At low strains G′ and G″ at 1 Hz are independent of the applied strain corresponding to linear behaviour. However at larger strains the suspensions start to yield and the viscoelastic moduli no longer reflect the intrinsic suspension rheology, as they depend strongly on the applied strain. The yield values of the strain (and stress) indicate the departure from elastic behaviour and the beginning of irreversible deformation. In Figure 4 it can be observed that the elastic modulus G′ as a function of strain fits well to the curve represented by Equation 2.

The three calculated values of the apparent yield stress as a function of particle dry mass fraction w are plotted in Figure 5. For all the suspensions the yield stress, obtained from both flow and oscillatory measurements, increased with the dry mass fraction w independently of the type of plant material and the particle shape. The correlation between both parameters σy and w was calculated using a power-law model $\sigma_y = aw^b$. The resulting fitted constants a and b are listed in Table 3. The power law behaviour fitted well for most of the different suspensions with a R^2 above 0.9. The deviations observed between measured and fitted values, in for example the suspension containing carrot cell fragments, are likely due to the experimental errors which might be present when measuring the yield stress of this type of system. These errors include slip, which although it will be reduced using a vane geometry it will still be present. Furthermore the shear rate might show an irregular (or at least non-uniform) profile using a wide gap vane, decreasing from the blade tips across the gap and might even be zero in the outer portion of the gap. The fluid within the blades is assumed to rotate along with them so it

Table 2 Flow indices, obtained by fitting the up and return flow curves to the Hershel-Bulkley model. Values are shown for the highest and lowest concentration samples in each data series. It is expected that the return curves provide more reliable values for the index, as the fit to the model is much better in these cases

	Flow index Herchel-Bulkley up	Flow index Herchel-Bulkley return
Carrot cell clusters w 0.015	0.74±0.01	0.31±0.05
Carrot cell clusters w 0.044	0.43±0.04	0.27±0.01
Carrot cell fragments w 0.022	0.63±0.02	0.20±0.03
Carrot cell fragments w 0.063	0.29±0.03	0.23±0.02
Tomato individual cells w 0.014	0.77±0.03	0.34±0.04
Tomato individual cells w 0.036	0.60±0.01	0.21±0.01
Tomato cell fragments w 0.015	0.49±0.03	0.296±0.002
Tomato cell fragments w 0.035	0.54±0.02	0.25±0.01

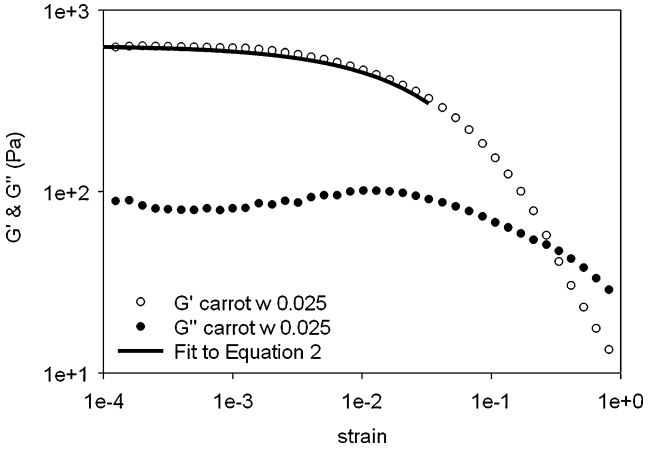

Fig. 4 Typical oscillatory shear measurements at a frequency of 1 Hz of the storage modulus G′ (closed symbols) and loss modulus G″ (open symbols) as a function of the strain for a suspension of carrot cell clusters with a dry mass fraction of 0.025. Solid line represents the fitting to Equation 2

generates a cylindrical surface with a radius similar to that of the vane; however in these suspensions (containing large anisotropic particles) some particles might be sheared also between the vane blades, leading also to anomalous shear rate measurements.[9]

All suspensions showed values of the b exponent around 3±0.55, the only exception was the yield stress calculated form return flow curves of the carrot cell fragments: the exponent in this case was lower, at 1.9, however the quality of the fitting, R^2 below 0.9, was poor for this calculated yield stress. The similar b exponent obtained for the two materials and the different particle shapes could indicate that the type of network structure is also similar.

The elastic modulus G′ from oscillatory experiments is plotted as a function of w in Figure 6, where it can be observed that it also followed a power-law behaviour with a R^2 above 0.98. The b exponent depended on the plant type: for the carrot suspensions it was approximately 3 and for tomato suspensions 4 (Table 4). While suspensions of carrot fragments clearly showed lower elastic moduli G′ compared to cell clusters, the G′ of the tomato individual cells and cell fragments was similar, albeit slightly higher for the fragments.

Yield Strain

The yield strain values calculated from oscillatory curves are plotted as a function of the dry mass fraction w in Figure 7. The measured yield strain values were very low

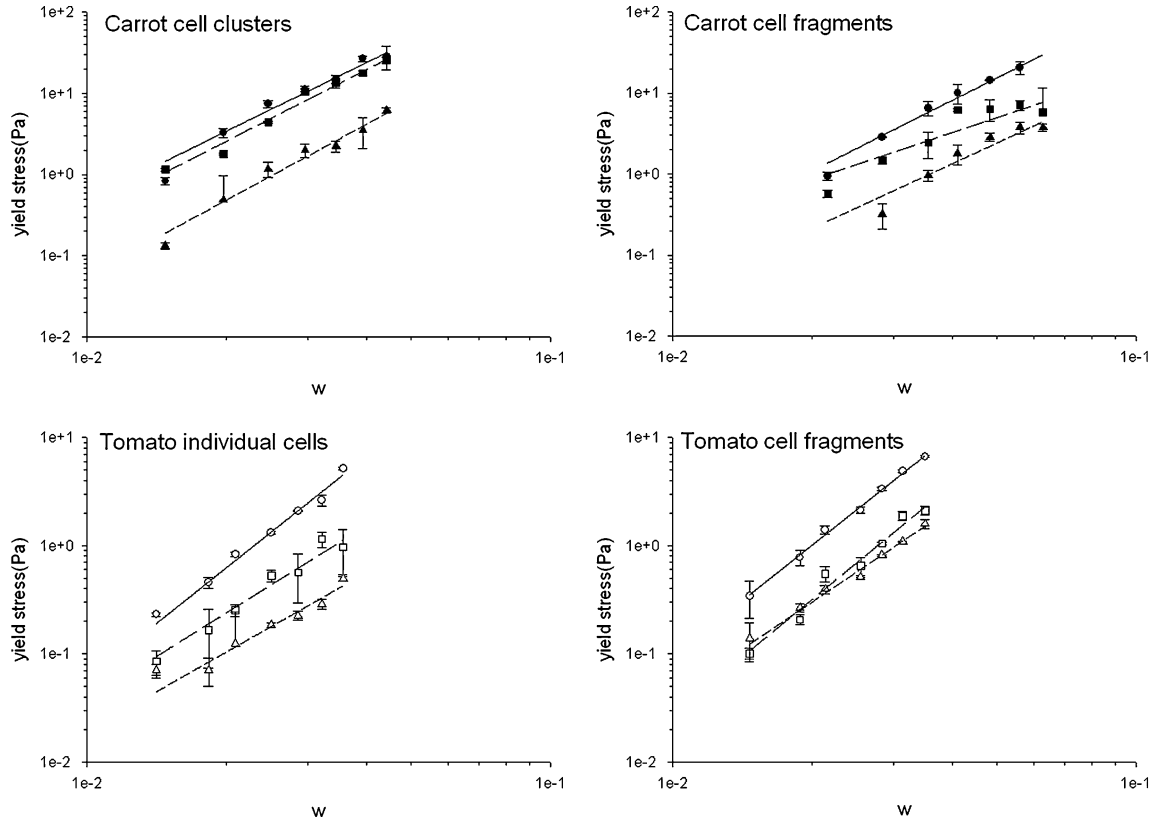

Fig. 5 Log-log plot of yield stress obtained by fitting the Hershel-Bulkley (HB) model to flow up-curves (circles), flow return-curves (squares) and from oscillatory measurements (triangles) of carrot (closed symbols) and tomato (open symbols) suspensions against dry mass fraction w. The solid and dashed lines represent the power-law fit. Error bars represent the standard deviation of three measurements

Table 3 Power-law fit for the yield stress as a function of dry mass fraction w. Herschel-Bulkley yield stress calculated from up curves (up HB σy), from return curves (return HB σy) and from oscillatory measurements (osc σy)

	up HB $\sigma y = aw^b$			return HB $\sigma y = aw^b$			osc $\sigma y = aw^b$		
	a/Pa	b	R^2	a/Pa	b	R^2	a/Pa	b	R^2
Carrot clusters of cells	2×10^{-5}	2.80	0.97	2.4×10^{-5}	2.92	0.98	0.9×10^{-5}	3.09	0.97
Carrot cell fragments	0.9×10^{-5}	2.88	0.99	0.1×10^{-4}	1.90	0.83	0.7×10^{-4}	2.64	0.92
Tomato individual cells	3.9×10^{-5}	3.41	0.97	0.8×10^{-5}	2.67	0.93	0.1×10^{-4}	2.43	0.94
Tomato cell fragments	6×10^{-5}	3.40	0.99	3×10^{-5}	3.51	0.97	0.2×10^{-5}	2.88	0.99

for all the samples. All the suspensions showed a decrease in yield strain γ_y as a function of dry mass fraction w; this trend being opposite to that obtained for the yield stress. The yield strain did not follow a power-law behaviour with dry mass fraction. The concentration dependency was less significant for the suspension of carrot cell clusters, which showed the lowest yield strain values of all systems, in the range 0.0018–0.002. The cell fragments showed higher yield strain values than the clusters and the single cells. It was not possible to accurately calculate a yield strain for suspensions with a dry mass fraction below 0.015 and 0.021 for carrot cell clusters and carrot cell fragments respectively. For tomato it was not possible below a dry mass fraction of 0.018 for individual cells and 0.015 for suspensions of cell fragments. The reason being that either these suspensions did not show a significant G′ or the oscillatory measurements were not reproducible.

Discussion

The observed increase in viscosity with particle concentration in the suspensions is due to the disturbance of the flow field due to the presence of particles. Furthermore squeezing flow between particles, when they move relative to one another, will increase the viscous dissipation, especially in concentrated systems.[12] Furthermore it was observed that the viscosity did not continue to increase at the same rate with increasing dry mass fraction.

The yield stress, σ_y, is defined as the minimum stress that needs to be applied to a material before flow will occur or in other words the stress corresponding to the transition from elastic to plastic deformation.[1] The existence of a true yield stress is controversial[13] however it is considered one of the most relevant parameters to determine the flow properties of any material. While the yield stress depends primarily on the volume of the suspension occupied by the particles, this volume depends on particle properties such as size distribution, morphology and interparticle forces. In this work the generated suspensions, characterised by certain particle shapes, were polydisperse in size and morphology. Similar polydispersity has been broadly reported in the literature for dispersions generated from fresh plant material and using conventional food processes.[14,15] In the literature the effect of polydispersity on the rheological properties has been studied on model systems containing spherical particles, where a multimodal system showed lower viscosities than a similar monomodal suspension[16] and a theory to predict how polydispersity affects packing of spherical particles has been recently developed.[17] It has also been pointed out that in suspensions of polydisperse non spherical particles, like the ones

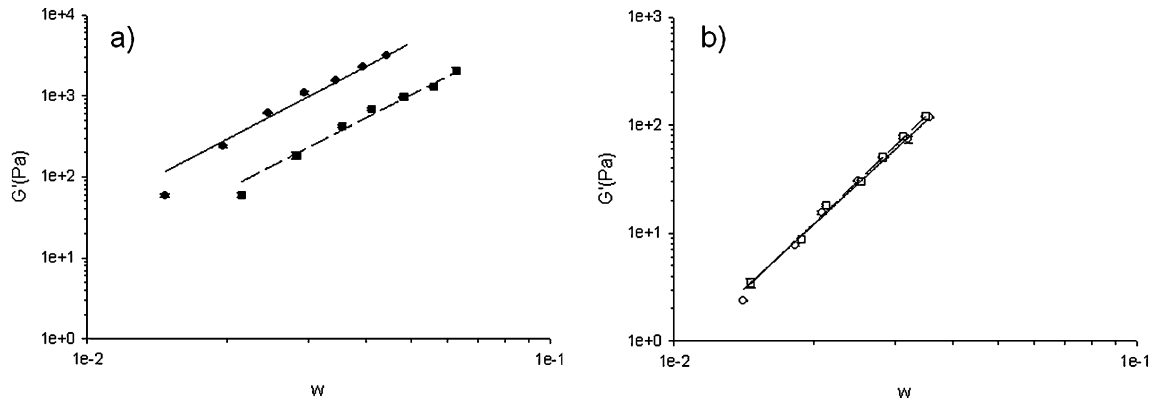

Fig. 6 G′ as a function of dry mass fraction w. **a** Carrot suspensions containing cell clusters (circles) and fragments (squares) and (**b**) tomato suspensions containing individual cells (circles) and cell fragments (squares)

Table 4 Power-law fit for the elastic modulus G′ as a function of dry mass fraction w

	$G' = aw^b$		
Sample	a/Pa	b	R^2
Carrot cell clusters	3.5×10^7	2.99	0.99
Carrot cell fragments	6.5×10^6	2.92	0.99
Tomato individual cell	6.1×10^7	3.95	0.99
Tomato cell fragments	11×10^7	4.10	0.99

in this work, parameters such as the shapes, aspect ratio and surface roughness must be taken into account as they influence the maximum packing fraction and the interactions between particles under static and flow conditions.[18]

The lower yield stress values calculated from return flow curves could indicate that once the original structure is lost it is not immediately recovered. The yield stress obtained from oscillatory experiments showed the lower values, but differences in absolute values (as opposed to trends with dry mass fraction w) have little significance as the analysis is different in the two types of measurement. The yield stress, and also the elastic moduli G′, increased with particle concentration for all suspensions. At lower dry mass fraction w both carrot suspensions showed similar apparent yield stresses, however at higher dry mass fractions the cell fragments clearly showed lower yield stress values. Considering that the cell fragments have a higher aspect ratio than cell clusters they might pack less efficiently leading to higher yield stress values. The change in particle shape, and presumably in flexibility, could explain the differences in yield stress, however as described above it should also be considered that particle size and particle size distribution are different and therefore the combination of all these parameters will result in different rheological properties. In contrast to carrot, the yield stress of the tomato cell fragments was larger than the single cells for the whole range of dry mass fraction studied, even for the lower dry mass fractions. There was also a slight increase in the G′ values of the suspensions containing tomato cell fragments. Similar enhancement of the rheological parameters has been previously reported for tomato cell fragments.[8,19] This could be due to the open structure of the tomato cell walls which might lead to polymer interactions, via physical entanglements and perhaps other attractive forces such as electrostatic interactions. An increase in the degree of cell wall disruption by high pressure homogenisation (Figure 1d) would increase the particle interactions producing a stronger network and increasing the apparent yield stress of the suspensions. An increase in particle concentration in the suspensions will increase both elastic and attractive interactions between particles, leading to a larger yield stress.

The power law scaling of the yield stress with particle concentration was characterised by an exponent ‘b’of around 3 for all plant suspensions studied, independently of the plant origin and particle shape. Power law exponents of 2.5 for tomato individual cells and 2 for cell fragments have been reported in the literature for the yield stress as a function of water insoluble solids.[19] These values lie within the range of the reported power-law indices of between 2.5 and 4.4 for flocculated suspensions[20] and wood suspensions[21] investigated as a function of particle volume fraction. Note that our analyses are in terms of dry mass fraction w, but the (unknown) constant of proportionality between w and volume fraction has no effect upon the exponent b. The exponent we find of $b=3$ seems to be also in agreement with the values obtained in the literature for strongly flocculated dispersions of colloidal particles (spheres, plates and rods), which showed a power-law behaviour for the shear yield stress described by $\sigma_y \sim \phi^{2.5-3}a^{-2}$ where a is the radius of the smaller particle.[22,23]

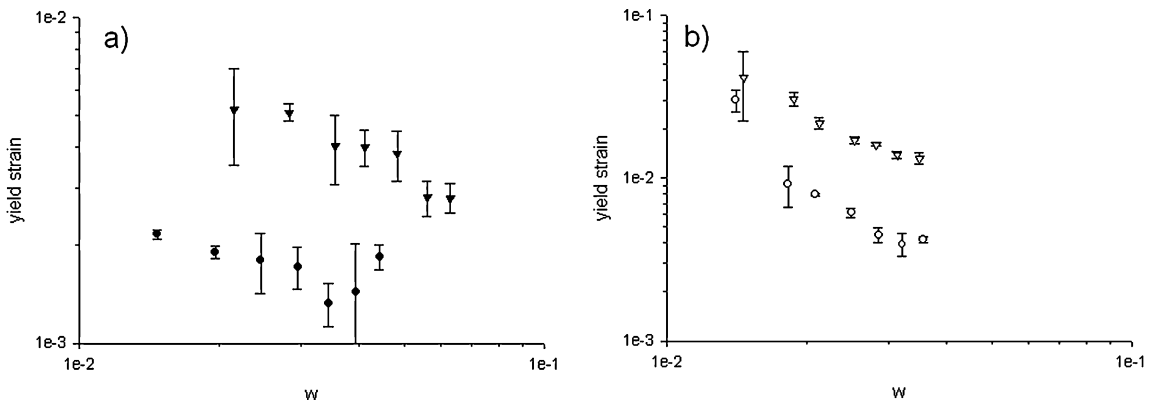

Fig. 7 Yield strain obtained from oscillatory curves as a function of dry mass fraction w. **a** Carrot cell clusters (circles) and cell fragments (triangles) and (**b**) tomato individual cells (circles) and cell fragments (triangles). Notice that the vertical scale for tomato samples is ten times that for carrot samples

These systems were described as networks which have a heterogeneous structure comprising a collection of interconnected fractal aggregates, while in our systems, there was no evidence from the micrographs for a fractal or self-similar structure.

The power law indices obtained for G′ were 3 for carrot cell clusters and fragments, and 4 for tomato individual cells and fragments. For carrot cell clusters and individual cells, power-law exponents of 3 and 6 have been reported.[24] The value 4 has been obtained for aggregate networks of colloidal particles[22] and this same value was predicted for such networks assuming that they are fractal.[25] In the work of Bayod et al [26] tomato suspensions were assumed to behave as fractal networks,[26] and this implies a fractal dimension of the network of 2.67≤Df≤2.85, based on the theoretical prediction $G' \propto \phi^{1/(3-Df)}$ for such networks. However, as noted above, it seems unlikely that such dense systems could contain self-similar structures over any significant range of length scales; a conclusion supported by microscopy. Furthermore, such fractal models are poorly predictive, being consistent with a wide range of exponents 'b', depending on the fractal dimension of the constituent clusters.

As an alternative, we suggest here another mechanism for generating the elastic modulus, which appears to be a more plausible explanation for the observed power law dependence, and is supported qualitatively by microscopy[2] We consider that the plant cell wall material consists of thin elastic sheets, with thickness t, and Young's modulus Y (Figure 8). These sheets then become folded in order to fit into the required space available. In principle, the folding may happen in a three-dimensional manner, like crumpled sheets of paper[30], with the stored elastic energy dominated by stretching ridges[31]. However, microscopy images of highly compressed plant material suspensions[2] suggest that actually the folding occurs in a much more two-dimensional manner, which is shown schematically in Figure 8, and which we analyse here.

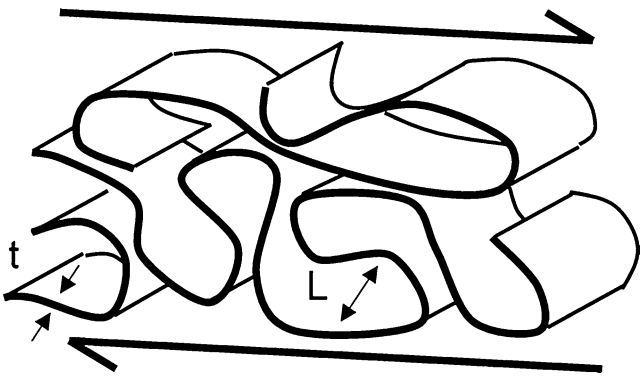

Fig. 8 Schematic picture of a folding sheet structure. L is the typical separation of junctions or contacts between sheets and t the thickness of the sheet. For simplicity, the sheets are shown aligned with the shear field, but this is not a necessary part of the model

Since Figure 8 is highly schematic, it is important to note what features we are trying to capture. The principal idea is that the elastic sheets fold like ribbons, so that their deformation is primarily around one axis of curvature at each point. Put another way, the Gaussian curvature is much smaller than the mean curvature. For an intact cell, which already has Gaussian curvature by virtue of its convex shape, and which can only be deformed by stretching or crumpling[32] (producing several points of high Gaussian curvature[31]), this will not be true. Therefore the assumption of ribbon-like folding is only likely to be valid if the pieces of cell wall material are indeed ribbon-like (being of longer length than width), or if the processing has created tears in the rounded walls of the cells, again allowing for this type of deformation. There is evidence from micrographs that this kind of simple, folded structure is the type of deformation encountered in processed cell wall materials above close packing[2].

In Figure 8, we have, for ease of viewing, presented the ribbons as being aligned relative to the direction of shear (more specifically, they have been drawn such that at every point, the normal to the ribbon surface is perpendicular to the vorticity direction). This is not a necessary assumption in our model: the sheets may be much less aligned, provided shear deformation of the structure as a whole can be accommodated through further ribbon-like deformation of the constituent sheets.

The second requirement of the model is that the sheets are not free to slide over one another: either through friction or attractive interactions, where two sheets touch, they are pinned, or constrained not to move relative to one another. We refer to these locations as "elastic entanglements", although they are more likely to be produced by surface forces, rather than knots or similar topological constraints (this is in contrast to polymer theory, where topology is what produces elastic contraints).[33,34]

The other requirements of the model are that the sheets themselves are elastic under small bending deformation, and (as is to be expected) cannot pass freely through one another. We also assume that the easiest mode of deformation is for the sheets to bend, rather than to stretch, as discussed below.

Starting from these assumptions, and considering the manner in which space is filled by these sheets in Figure 8, the volume fraction occupied by one portion of a sheet between entanglements in the total volume would be

$$\phi \sim \frac{hLt}{L^2 h} \sim \frac{t}{L} \tag{6}$$

where L is the distance between elastic entanglements of the sheets, and h is the depth of the structure (which cancels

out). This is easiest to see in the case of aligned ribbons (Figure 8), but the final scaling will apply also in the non-aligned case. As noted above, these entanglements are regions where two sheets meet each other, and (due to friction for example), are not free to slide past one another. The actual size of the sheets may (and especially at higher volume fraction, will) be larger than L, since a single sheet may fold back on itself and encounter several elastic entanglements.

If the resulting network is sheared, and the deformation of all the material is affine, so all the sheets are stretched rather than bend (as might occur for a very dense network with a volume fraction close to unity), then it is clear that the elastic modulus will be given approximately by $G' \sim Y\phi$, with a pre-factor of order unity to convert the Young modulus into a shear modulus. However, at lower phase volumes, it is likely that the network will deform principally via bending of the elastic sheets, as is known to occur in networks of semi-flexible, non-thermal rods[35].

Consider therefore one section of the network, as shown in Figure 9, being deformed through a strain γ. We imagine that the structure has a depth h into the page (which will eventually cancel out of the analysis). Again, the assumption of alignment of sheets is used for simplicity of analysis, but we expect the same scaling to result from an un-aligned collection of sheets also.

In the deformed state (Figure 9), the elastic energy stored in this part of the network (which has a volume of L^2h) is given by

$$E \sim hLY\frac{1}{R^2}t^3 \tag{7}$$

Where Y is the young modulus and R the radius of curvature, which is given roughly by $R \sim L/\gamma$.

Thus the total energy stored is

$$E \sim \frac{hLYt^3\gamma^2}{L^2}, \tag{8}$$

where γ is the shear strain.

Now for a material with shear modulus G′ the energy stored per unit volume under shear strain would be

$$U(\gamma) = \frac{1}{2}G'\gamma^2. \tag{9}$$

Since for our systems we know

$$U(\gamma) \equiv \frac{E}{L^2h} \sim \frac{Yt^3\gamma^2}{L^3} \tag{10}$$

then from Equations 9 and 10

$$G' \sim \frac{Yt^3}{L^3} \tag{11}$$

and so from Equations 11 and 6, we obtain our final result

$$G' \sim Y\phi^3. \tag{12}$$

The predicted exponent 3 for the scaling of G′ agrees well with the one obtained for the studied suspensions of carrot particles indicating that they could behave as folding sheets. The expected values for affine deformation ($G' \sim Y\phi^1$) and bending of elastic rods ($G' \sim Y\phi^2$, from a similar analysis to that above) give exponents b that are clearly lower than those obtained in our studies.

Turning now to yield strain, the minimum yield strains measured for each system indicates that the suspensions yield for relative particle displacements of much less than one diameter (i.e. strains much less than 1) (Table 1). The yield strain values for the suspensions were of the order of the reported values for high phase volume polydisperse emulsions: ~0.1% strain.[28] This could indicate that in these systems, even though other effects might take place, it is mainly the polydispersity which is responsible for the low yield strain values.[29] For both plant material sources, suspensions of cell fragments showed higher yield strain values than clusters and individual cells. This increase in yield strain values could be due to an increased aspect ratio, which might permit greater contact between adjacent particles increasing mechanical linkages and therefore leading to yield at larger strains. In the case of tomato fragments this could be enhanced by a higher possibility for polymer entanglements between particles, which are likely to be able to withstand large deformations. The yield strain decreased with particle concentration, and similar behaviour was found in the literature for

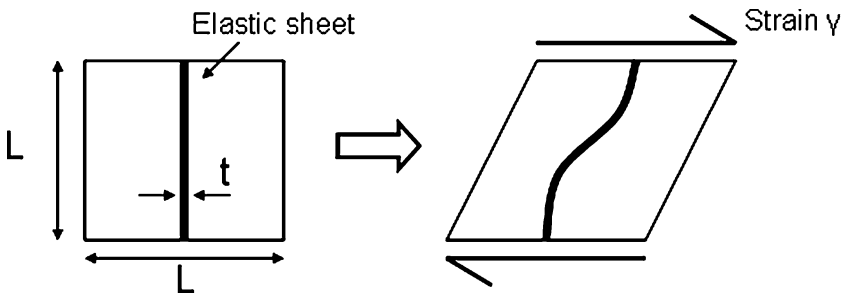

Fig. 9 Schematic picture of one element of the network in Figure 8, consisting of a portion of an elastic sheet between two junctions, being deformed through a strain γ, and accommodating this strain through bending

strongly flocculated dispersions of colloidal particles.[22,27] The decrease in γ_y at increased amounts of cell fragments could be due to some of these rod-like particles deforming to lower aspect ratio morphologies and in the case of tomato as the concentration of the particles increases the polymers may be forced to collapse onto the cell surfaces, reducing the scope for entanglements and hence leading to systems with lower yield strains. Further work is required to understand the dependence of yield strain on particle concentration.

Conclusions

Suspensions of micrometer sized plant particles with a range of different shapes: cell clusters, individual cells and cell fragments showed a rheological behaviour characterised by an apparent yield stress followed by shear-thinning for a range of dry mass fractions. The yield stress, calculated by fitting to a Herschel-Bulkley model and from oscillation measurements, increased with particle concentration following a power-law behaviour. The power law exponent of approximately 3±0.5 for all suspensions could indicate a similar type of network, independently of the plant origin and particle shape. The power law fitting of the linear elastic modulus G′ with dry mass fraction w showed values of the exponent of 3 for carrot and 4 for tomato suspensions. For all the suspensions the yield strain, calculated from oscillatory measurements, decreased with dry mass fraction and had values below 1% strain. Our results show that the suspension of plant particles studied have similar behaviour to flocculated suspensions of colloidal particles, but we also suggest an explanation for the exponent of G′ versus w, based upon a non-affine network of folded elastic sheets, which seems more plausible, given the observed microstructure of these systems.

Acknowledgements We thank Mr. Vishmai Chapara for his assistance with sample preparation and rheological measurements. Dr Stephan Schumm is greatly acknowledge for useful discussions and proof reading of the manuscript.

The authors gratefully acknowledge financial support from the European Commission FOOD-2004-T5.4.1.3: Project 023115-Healthy Structuring.

References

1. H.A. Barnes, J.F. Hutton, K. Walters, *An Introduction to Rheology* (Elsevier, Amsterdam, 1994), p. 169
2. P. Lopez-Sanchez, V. Chapara, S. Schumm, R. Farr, Shear elastic deformation and particle packing in plant cell dispersions. (Submitted J Food Biophysics)
3. C.W. Macosko, *Rheology: Principles, Measurements and Applications* (VCH, New York, 1994), pp. 425–474
4. C. Servais, R. Jones, I. Roberts, The influence of particle size distribution on the processing of food. J. Food Eng. **51**, 201–208 (2002)
5. C. Gallegos, J.M. Franco, P. Partal, Rheology of food dispersions. Rheology reviews. 19–65 (2004).
6. D.B. Genovese, J.E. Lozano, M.A. Rao, The rheology of colloidal and non-colloidal food dispersions. Review. J. Food Sci. **72**, R11–R20 (2007)
7. M.A. Rao, C.G. Qiu, Rheological properties of plant food dispersions. *ACS symposium series*, *American Chemical society* pp. 149–171 (1989)
8. P. Lopez-Sanchez, J. Nijsse, H.C.G. Blonk, L. Bialek, S. Schumm, M. Langton, Effect of mechanical and thermal treatments on the microstructure and the rheological properties of carrot, broccoli and tomato dispersions. J. Sci. Food Agric. **91**, 207–217 (2011)
9. Q.D. Nguyen, D.V. Boger, Yield stress measurement for concentrated suspensions. J. Rheol. **27**, 321–349 (1983)
10. B. Derakhshandeh, S.G. Hatzikiriakos, C.P.J. Bennington, The apparent yield tress of pulp fibre suspensions. J. Rheol. **54**, 1137–1154 (2010)
11. P. Lopez-Sanchez, C. Svelander, L. Bialek, S. Schumm, M. Langton, Rheology and microstructure of carrot and tomato emulsions as a result of high-pressure homogenisation conditions. J. Food Sci. **76**, 130–140 (2011)
12. J. Mewis, Flow behaviour of concentrated suspensions: predictions and measurements. Int. J. Miner. Process. **44–45**, 17–27 (1996)
13. H.A. Barnes, The 'yield stress myth?' paper—21 years on. Appl. Rheol. **17**, 43110–1–43110–5 (2007)
14. B. Yoo, M.A. Rao, Effect of unimodal particle-size and pulp content on rheological properties of tomato puree. J. Texture Stud. **25**, 421–436 (1994)
15. F.W.C. den Ouden, T. van Vliet, Particle size distribution in tomato concentrates and effects on rheological properties. J. Food Sci. **62**, 565–567 (1997)
16. R.J. Farris, Prediction of the viscosity of multimodal suspensions from unimodal viscosity data. Trans. Sot. Rheol. **12**, 281–301 (1968)
17. R.S. Farr, R.D. Groot, Close packing density of polidisperse hard spheres. J. Chem. Phys. **131**, 244104 (2009)
18. A.B. Metzner, Rheology of suspensions in polymeric liquids. J. Rheol. **29**, 739–775 (1985)
19. E. Bayod, P. Mansson, F. Innings, B. Bergenstahl, E. Tornberg, Low shear rheology of concentrated tomato products: effect of particle size and time. Food Biophys. **2**, 146–157 (2007)
20. E. van der Aershot, J. Mewis, Equilibrium properties of reversible flocculated dispersions. Colloid Surface **69**, 15–22 (1992)
21. C.P.J. Bennington, R.J. Kerekes, J.R. Grace, The yield stress of fibre suspensions. Can. J. Chem. Eng. **68**, 748–757 (1990)
22. R. Buscall, I.J. Mcgowan, P.D.A. Mills, R.F. Stewart, D. Sutton, L.R. White, G.E. Yates, The rheology of strongly-flocculated suspensions. J. Non-Newtonian Fluid Mech. **24**, 183–202 (1987)
23. R. Buscall, P.D.A. Mills, J.W. Goodwin, D.W. Lawson, Scaling behaviour of the rheology of aggregate networks formed from colloidal particles. J. Chem. Soc. Faraday Trans. I. **84**, 4249–4260 (1988)
24. L. Day, M. Xu, S.K. Øiseth, L. Lundin, Y. Hemar, Dynamic rheological properties of plant cell wall particle dispersions. Colloids Surf. B Biointerfaces **81**, 461–467 (2010)
25. W.D. Brown, R.C. Ball, Computer simulation of chemically limited aggregation. J. Phys. A. **18**, L517–L521 (1985)
26. E. Bayod, E. Tornberg, Microstructure of highly concentrated tomato suspensions on homogenisation and subsequent shearing. Food Res. Int. doi: 10.1016/j.foodres.2011.01.005 (2011).
27. S.S. Narine, A.G. Marangoni, Mechanical and structural model of fractal networks of fat crystals at low deformations. Phys. Rev. E. **60**, 6991–7000 (1999)
28. H.M. Princen, A.D. Kiss, Rheology of foams and highly concentrated emulsions: IV. An experimental study of the shear

viscosity and yield stress of concentrated emulsions. J. Colloid Interface Sci. **128**, 176 (1989)
29. T.G. Mason, J. Bibette, D.A. Weitz, Yielding and flow of monodispersed emulsions. J. Colloid Interface Sci. **179**, 439–448 (1996)
30. G.A. Vliegenthart, G. Gompper, Forced crumpling of self-avoiding elastic sheets. Nat. Mater. **5**, 216–221 (2006)
31. A. Lobkovsky, S. Gentges, H. Li, D. Morse, T.A. Witten, Scaling properties of stretching ridges in a crumpled elastic sheet. Science **270**, 1482–1485 (1995)
32. A. L. Cauchy, J. Ec. Polytech., XVIe cahier, IX, **87** (1813).
33. P.G. de Gennes, Reptation of a polymer chain in the presence of fixed obstacles. J. Chem. Phys. **55**(2), 572 (1971)
34. M. Doi, S.F. Edwards, Dynamics of concentrated polymer systems. 2. Molecular motion under flow. J. Chem. Soc. Faraday Trans 2 **74**, 1802 (1978)
35. D.A. Head, A.J. Levine, F.C. MacKintosh, Distinct regimes of elastic response and deformation modes of cross-linked cytoskeletal and semiflexible polymer networks. Phys. Rev. E. **68**, 061907 (2003)